

Local structural origins of the distinct electronic properties of Nb-substituted SrTiO_3 and BaTiO_3

Katharine Page,¹ Taras Kolodiaznyy,² Thomas Proffen,³ Anthony K. Cheetham,⁴ and Ram Seshadri¹

¹*Materials Department, University of California, Santa Barbara, CA 93106, USA*

²*National Institute for Materials Science, 1-1 Namiki, Tsukuba, Ibaraki, 305-0044 Japan*

³*Los Alamos National Laboratory, Lujan Neutron Scattering Center, MS H805, Los Alamos, NM 87545, USA*

⁴*Department of Materials Science and Metallurgy, University of Cambridge, CB2 3QZ, UK*

Near or less than 10% Nb substitution on the Ti site in perovskite SrTiO_3 results in metallic behavior, in contrast to what is seen in BaTiO_3 . Given the nearly identical structure and electron counts of the two materials, the distinct ground states for low substitution have been a long-standing puzzle. Here we find from neutron studies of average and local structure, the subtle yet critical difference that we believe underpins the distinct electronic properties in these fascinating materials. While $\text{SrTi}_{0.875}\text{Nb}_{0.125}\text{O}_3$ possesses a distorted non-cubic structure at 15 K, the BO_6 octahedra in the structure are regular. $\text{BaTi}_{0.875}\text{Nb}_{0.125}\text{O}_3$ on the other hand shows evidence for local cation off-centering whilst retaining a cubic structure.

PACS numbers: 61.05.F, 77.84.Dy, 71.30.+h

Small substitutions of Nb for Ti in the perovskite SrTiO_3 give rise to electronic conductivity,[1, 2] and even superconductivity.[3] Nb-substituted SrTiO_3 is widely used as a conducting substrate for epitaxial perovskite thin films. BaTiO_3 which has a ferroelectric ground state,[4] also substitutes Nb on the Ti site, and is known to form almost a complete solid solution with BaNbO_3 . Despite possessing the same cubic perovskite structure, depicted in Fig.1(a), (at least for greater than 10 atom-% substitution) and identical electron counts, the Sr compounds display metallic behavior while the Ba compounds are localized up to at least 20% substitution.[5]

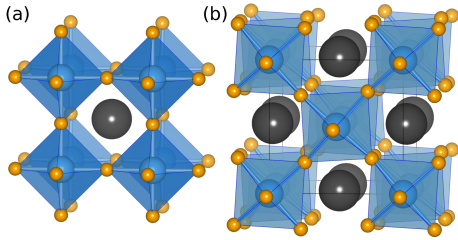


FIG. 1: (Color online.) Crystal structures of SrTiO_3 at (a) room temperature when it is cubic, and (b) at low temperatures when it is tetragonal. The structural parameters used to depict (b) were obtained from Rietveld refinement of the 15 K neutron diffraction data of $\text{SrTi}_{0.875}\text{Nb}_{0.125}\text{O}_3$.

In order to unravel the possible structural underpinnings of the distinct behavior of the end-members in this solid solution series, we have prepared sample compositions with 12.5% Nb-substitution: $\text{SrTi}_{0.875}\text{Nb}_{0.125}\text{O}_3$ (STNO) and $\text{BaTi}_{0.875}\text{Nb}_{0.125}\text{O}_3$ (BTNO), and studied their average and local structures using time of flight neu-

tron diffraction measurements.

Samples were prepared from high purity (99.99%) $\text{Ba}(\text{Sr})\text{CO}_3$, TiO_2 and Nb_2O_5 powders purchased from Sigma Aldrich. Pellets of stoichiometric amounts of the starting materials were calcined at 1100°C for 20 h in flowing H_2 , at a flow rate of $50\text{ cm}^3/\text{min}$, with a second regrinding/repelletization at 1350°C for 20 h in flowing H_2 . Four-probe resistivity was measured on 95% dense ceramic samples cut into $2 \times 2 \times 9\text{ mm}^3$ parallelepipeds. Magnetic susceptibility in the 2 K to 400 K range was measured with a QD MPMS XL magnetometer. High- Q resolution neutron powder diffraction data were collected on the $\text{SrTi}_{0.875}\text{Nb}_{0.125}\text{O}_3$ and $\text{BaTi}_{0.875}\text{Nb}_{0.125}\text{O}_3$ samples on the NPDF instrument at the Los Alamos National Laboratory Lujan Neutron Scattering Center[6] at room temperature and at 15 K. Rietveld refinement of the diffraction data was carried out in the GSAS-EXPGUI[7] suite of programs. The experimental pair distribution function was extracted from neutron total scattering data using the program PDFGETN.[8] The wavevector cutoff Q_{max} used for the transform was 40 \AA^{-1} . PDF refinements were carried out using the PDFGUI program.[9]

The distinct properties are amply illustrated by considering the temperature dependence of the electrical resistivity and the magnetic susceptibility of the solid solution series $\text{Sr}_{1-x}\text{Ba}_x\text{Ti}_{0.9}\text{Nb}_{0.1}\text{O}_3$ displayed in the panels of Fig. 2. As the value of x (the amount of Ba) is increased across the solid solution, the resistivity (Fig. 2a) displays an upturn at low temperatures; the change from a positive to negative temperature coefficient of resistivity takes place between $x = 0.25$ and $x = 0.50$,

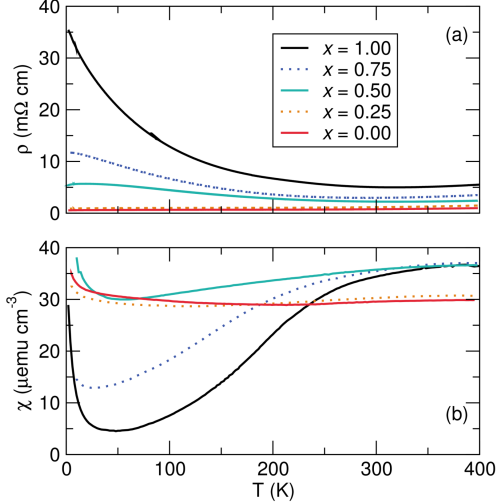


FIG. 2: (Color online.) Specific resistivity (a) and magnetic susceptibility (b) as a function of temperature for samples of $\text{Sr}_{1-x}\text{Ba}_x\text{Ti}_{0.9}\text{Nb}_{0.1}\text{O}_3$ demonstrate the metal-insulator transition as x increases. The data in (b) have not been corrected for atomic diamagnetism.

in a region where the resistivity values are somewhat smaller than the value suggested by Mott for the minimum conductivity.[10] In correspondence with electrical transport, the magnetic susceptibility of the Sr-rich side of the solid solution is largely temperature-independent, in keeping with its metallic transport properties, while the Ba-rich samples display a stronger temperature dependence, characteristic of moments on localized electrons. One explanation that has been proffered for the magnetic behavior is the formation of bipolarons.[11]

STNO and BTNO have very similar structures and lattice parameters. At room temperature, both compounds crystallize in the cubic perovskite $Pm\bar{3}m$ structure. Nb-substitution results in small expansion of the cell edge as expected from the 6-coordinate Shannon-Prewitt radii, as Ti^{4+} ($r = 0.61 \text{ \AA}$) is either substituted by Ti^{3+} ($r = 0.67 \text{ \AA}$), Nb^{5+} ($r = 0.64 \text{ \AA}$), or Nb^{4+} ($r = 0.68 \text{ \AA}$).[12] Rietveld refinement of time-of-flight neutron diffraction data confirms the average structures of both STNO and BTNO at room temperature are cubic. The only significant difference is in the cell parameters, with $a = 3.9237(1) \text{ \AA}$ and $a = 4.0147(1) \text{ \AA}$ respectively, in keeping with the much larger 12-coordinate radius of Ba^{2+} ($r = 1.61 \text{ \AA}$) compared with Sr^{2+} ($r = 1.44 \text{ \AA}$). Rietveld profile fits are displayed for STNO and BTNO at room temperature in Fig. 3a and Fig. 3c. At 15 K, BTNO remains cubic (Fig. 3d), while STNO transforms between 298 K and 15 K to the tetragonal $I4/mcm$ low temperature

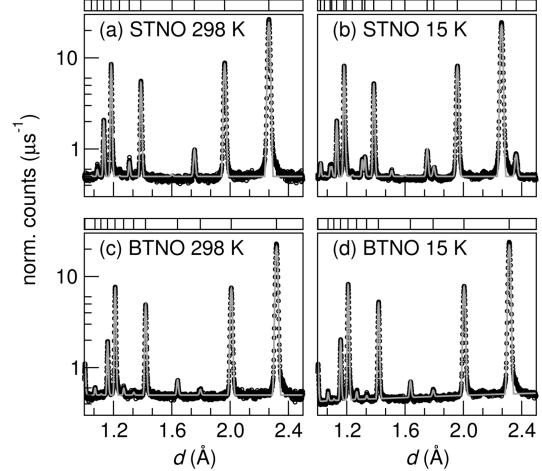


FIG. 3: A portion of the highest resolution bank of time-of-flight neutron diffraction data for $\text{SrTi}_{0.875}\text{Nb}_{0.125}\text{O}_3$ at (a) 298 K and (b) 15 K, and $\text{BaTi}_{0.875}\text{Nb}_{0.125}\text{O}_3$ at (c) 298 K and (d) 15 K. Circles are data and the lines are Rietveld fits to the cubic $Pm\bar{3}m$ structures for (a), (c), and (d), and to the tetragonal $I4/mcm$ structure for (b). Vertical lines at the top of each panel indicate expected peak positions. Note the log scale.

structure of SrTiO_3 (Fig. 3b).[13, 14] The structure is displayed in Fig. 1(b). In contrast to SrTiO_3 where the octahedral rotational order parameter at 20 K is 1.97° ,[14] the value obtained here for STNO at 15 K is $3.46(2)^\circ$. This larger value for the Nb-substituted compound reflects the slightly decreased tolerance factor.

Local structure was analyzed in terms of the atomic pair distribution function, $G(r)$, using $\text{A}_8\text{Ti}_7\text{NbO}_{24}$ supercells, as well as single-unit cell models with appropriate partial Ti/Nb occupancies. In Fig. 4, we compare the 15 K data and PDF fits to the average tetragonal structure of (a) $\text{SrTi}_{0.875}\text{Nb}_{0.125}\text{O}_3$ and the average cubic structure of (b) $\text{BaTi}_{0.875}\text{Nb}_{0.125}\text{O}_3$ to a maximum vector length of 50 \AA . Both compounds are remarkably well described by the average structures over this range, suggesting that local effects due to Nb-substitution are small. A $2 \times 2 \times 2$ perovskite supercell with Nb at the center and Ti at all corners, faces, and cell edges provided a model for probing whether the coordination of NbO_6 octahedra were distinct from those of TiO_6 octahedra. Within the resolution of these experiments, no differences were discernible, supporting the analysis using an average B -occupation unit cell. Results of the PDF refinement are displayed alongside results of the Rietveld refinement in Table I. Significant anomalies are found in the isotropic displacement parameters, U_{iso} for the two compounds. In $\text{SrTi}_{0.875}\text{Nb}_{0.125}\text{O}_3$ it is seen

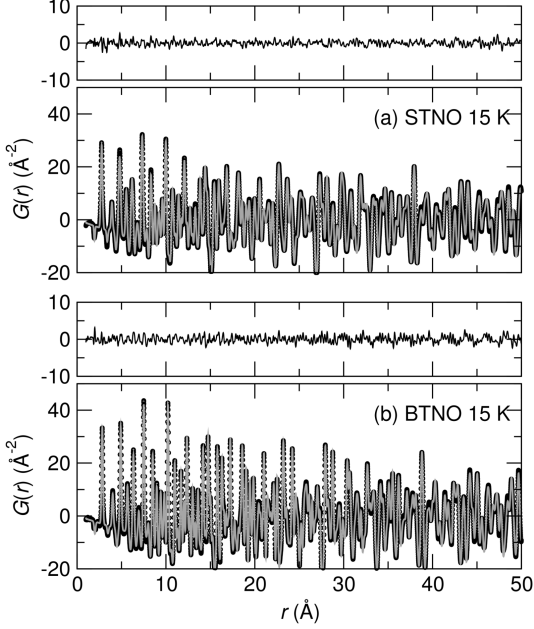


FIG. 4: Neutron pair distribution functions (PDF) of (a) $\text{SrTi}_{0.875}\text{Nb}_{0.125}\text{O}_3$ and (b) $\text{BaTi}_{0.875}\text{Nb}_{0.125}\text{O}_3$ acquired at 15 K. Circles are data and lines are fits to the average tetragonal (a) and cubic (b) structures. The difference between data and fit is displayed separately at the top of each panel.

at room temperature that U_{iso} is somewhat large on the *A* site (Sr) compared to the value found for Ba in $\text{BaTi}_{0.875}\text{Nb}_{0.125}\text{O}_3$. This is a signature of the tilting instability that drives the cubic compound to transform to a tetragonal ground state, whereupon all values of U_{iso} at 15 K are somewhat more reasonable.[4] In $\text{BaTi}_{0.875}\text{Nb}_{0.125}\text{O}_3$ on the other hand, it is the *B* site (Ti/Nb) that has an anomalously large U_{iso} , both at 300 K and at 15 K.

Figure 5 (a through d) displays the short r PDFs of $\text{SrTi}_{0.875}\text{Nb}_{0.125}\text{O}_3$ and $\text{BaTi}_{0.875}\text{Nb}_{0.125}\text{O}_3$ at room temperature and at 15 K. For $\text{BaTi}_{0.875}\text{Nb}_{0.125}\text{O}_3$ at 300 K and more markedly at 15 K, this first coordination shell is clearly bimodal. In contrast, the local structure of $\text{SrTi}_{0.875}\text{Nb}_{0.125}\text{O}_3$ is undistorted and well-described by the crystallographic model. The local distortion in $\text{BaTi}_{0.875}\text{Nb}_{0.125}\text{O}_3$ explains the larger *B*-site U_{iso} seen both in Rietveld and PDF results. This is the principal finding of this work, and points to a subtle yet fundamental difference in the local structures of these two compounds. To better understand the bimodal first (Ti/Nb)-O peak in the PDF of $\text{BaTi}_{0.875}\text{Nb}_{0.125}\text{O}_3$, we show alongside in Fig.5(e), simulations of the first peak PDF of BaTiO_3 in its different crystalline

structures: As it is cooled from high temperatures, BaTiO_3 transitions successively from cubic $Pm\bar{3}m$ to tetragonal $P4mm$ to orthorhombic $Amm2$ to, finally, it's rhombohedral $R\bar{3}m$ ground state.[4, 15] In the rhombohedral structure, Ti atoms in BaTiO_3 displace toward octahedral faces, resulting in three short and three long Ti-O distances, giving rise to a bimodal first peak in the PDF. This is precisely the situation in $\text{BaTi}_{0.875}\text{Nb}_{0.125}\text{O}_3$. However in BaTiO_3 local distortions are coherent and strain-coupled, and lead to phase transitions with associated changes in the average structure. In $\text{BaTi}_{0.875}\text{Nb}_{0.125}\text{O}_3$, the random substitution of Ti by 12.5-atom% Nb is sufficient to frustrate long-range ordering, and the quality of *cubic* refinements support the idea that displacements of (Ti/Nb) are very poorly correlated.

The results of this work underpin the differences in the local structures of $\text{SrTi}_{0.875}\text{Nb}_{0.125}\text{O}_3$ and $\text{BaTi}_{0.875}\text{Nb}_{0.125}\text{O}_3$ which draw from the distinct ground states of the undoped compounds. The introduction of random potentials *via* Nb-substitution

TABLE I: Average structures of $\text{SrTi}_{0.875}\text{Nb}_{0.125}\text{O}_3$ and $\text{BaTi}_{0.875}\text{Nb}_{0.125}\text{O}_3$ from Rietveld and 50 Å PDF refinement of time-of-flight neutron scattering data. Note the anomalously high U_{iso} for the A site in the strontium compound, relieved at 15 K *via* the phase transition to the tetragonal structure. The high U_{iso} for (Ti/Nb) for the barium compound remains at all temperatures. Refined parameters are shown with error.

$\text{SrTi}_{0.875}\text{Nb}_{0.125}\text{O}_3$				
	300 K, $Pm\bar{3}m$		15 K, $I4/mcm$	
	Rietveld	PDF	Rietveld	PDF
a (Å)	3.9237(1)	3.9255(1)	5.5391(2)	5.5418(4)
c (Å)			7.8312(4)	7.835(1)
$U_{iso}(\text{Sr})$ (Å ²)	0.0098(1)	0.0076(2)	0.0053(1)	0.0034(1)
$U_{iso}(\text{Ti/Nb})$ (Å ²)	0.0056(3)	0.0050(2)	0.0042(3)	0.0028(1)
$U_{iso}(\text{O})$ (Å ²)	0.0098(1)	0.0084(1)	0.0054(1)	0.0042(1)
$x(\text{O}2)$			0.2349(1)	0.2350(1)
occ.(Nb)	0.127(2)	1/8	0.123(2)	1/8
R_w (%)	3.6	7.7	3.8	7.7
$\text{BaTi}_{0.875}\text{Nb}_{0.125}\text{O}_3$				
	300 K, $Pm\bar{3}m$		15 K, $Pm\bar{3}m$	
	Rietveld	PDF	Rietveld	PDF
a (Å)	4.0147(1)	4.0165(1)	4.0084(1)	4.0100(1)
$U_{iso}(\text{Ba})$ (Å ²)	0.0061(1)	0.0052(3)	0.0028(1)	0.0021(1)
$U_{iso}(\text{Ti/Nb})$ (Å ²)	0.0093(3)	0.0080(2)	0.0070(2)	0.0059(1)
$U_{iso}(\text{O})$ (Å ²)	0.0077(1)	0.0061(1)	0.0053(1)	0.0040(1)
occ.(Nb)	0.131(1)	1/8	0.132(1)	1/8
R_w (%)	3.0	7.4	3.4	8.5

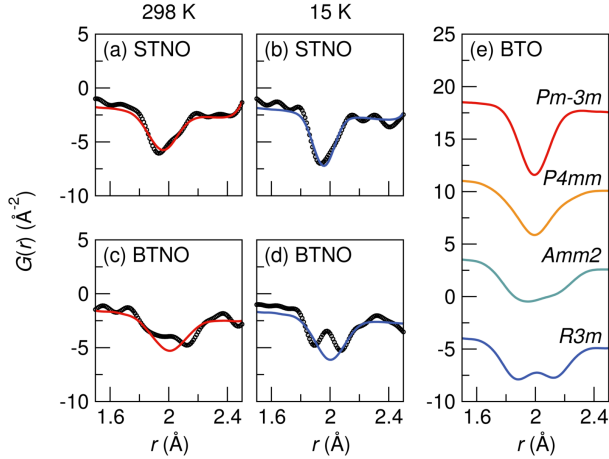


FIG. 5: (Color online.) Shortest (Ti/Nb)-O distances in the (a) 298 K PDF and (b) 15 K PDF of $\text{SrTi}_{0.875}\text{Nb}_{0.125}\text{O}_3$. Circles are experimental data and the lines are fits to the respective average structures. (c) and (d) show these distances for $\text{BaTi}_{0.875}\text{Nb}_{0.125}\text{O}_3$ at 298 K and 15 K respectively. (e) Calculated shortest Ti-O distances in BaTiO_3 for the different crystallographic modifications, using the structures of Kwei *et al.*[15] Note that the (Ti/Nb)-O distances are seen as negative peaks because of the negative neutron scattering length of Ti.

on the Ti site in BaTiO_3 , in addition to the introduction of charge carriers due to the aliovalent nature of the substitution, result in dipole-dipole correlations being rapidly suppressed. In particular, the role of charge carriers in bringing this about is dramatic. In systems where the substitution is isovalent, for example, $\text{BaTi}_{1-x}\text{Sn}_x\text{O}_3$, ferroelectricity is suppressed only somewhat slowly.[16] In keeping with ideas of “ferroelectric metals” (and their paucity), charge carriers screen the long-range electrostatic interactions responsible for ferroelectric order.[17, 18] However, local effects that are responsible for off-centering, namely the second-order Jahn-Teller distortion on Ti^{4+} , are quite robust to changing electron counts, and persist even when long-range ordering of dipoles has been suppressed. The precise relation between local off-centering and localized electronic ground states in $\text{BaTi}_{0.875}\text{Nb}_{0.125}\text{O}_3$ does not emerge from this study, except in that they suggest a means of lifting electronic degeneracy. In $\text{SrTi}_{0.875}\text{Nb}_{0.125}\text{O}_3$, where distortions are not found, there is no symmetry-derived mechanism for lifting the Ti/Nb t_{2g} electronic degeneracy.

We acknowledge helpful discussions with P. A. Pincus, P. B. Littlewood, and Chris Van de Walle. This work has benefited from the use of NPDF at the Lujan Center at Los Alamos Neutron Science Center, funded by the DOE Office of Basic Energy

Sciences. Los Alamos National Laboratory is operated by Los Alamos National Security LLC under DOE contract DE-AC52-06NA25396. The National Science Foundation is acknowledged for support in the form of a Graduate Student Fellowship to KP, a Career Award to RS (grant DMR04-49354), and for an upgrade of the NPDF instrument at Los Alamos (grant DMR00-76488). TK acknowledges MEXT for financial support.

- [1] F. Gervais, J.-L. Servoin, A. Baratoff, J. G. Bednorz, and G. Binnig, *Phys. Rev. B* 47 (1993) 8187–8194.
- [2] T. Tomio, H. Miki, H. Tabata, T. Kawai, and S. Kawai, *J. Appl. Phys.* 76 (1994) 5886–5900.
- [3] J. F. Schooley, W. R. Hosler, E. Ambler, J. H. Becker, M. L. Cohen, and C. S. Koonce, *Phys. Rev. Lett.* 14 (1965) 305–307.
- [4] H. D. Megaw, *Ferroelectricity in crystals*, Methuen, London, 1957.
- [5] J. F. Marucco, M. Ocio, A. Forget, and D. Colson, *J. Alloys Compounds* 262–263 (1997) 454–458.
- [6] Th. Proffen, T. Egami, S. J. L. Billinge, A. K. Cheetham, D. Louca and J. B. Parise, *Appl. Phys. A* 74 (2002) S163–S165.
- [7] A. C. Larson and R. B. Von Dreele, *General Structure Analysis System (GSAS)*, Los Alamos National Laboratory Report LAUR 86-748 (2000); B. H. Toby, *J. Appl. Crystallogr.* 34 (2001) 210–213.
- [8] P. F. Peterson, M. Gutmann, Th. Proffen and S. J. L. Billinge, *PDFGETN: J. Appl. Crystallogr.* 33 (2000) 1192.
- [9] C. L. Farrow, P. Juhas, J. W. Liu, D. Bryndin, E. S. Božin, J. Bloch, Th. Proffen, and S. J. L. Billinge, *J. Phys. Condens. Matter* 19 (2007) 335219(1–7).
- [10] N. F. Mott, *Metal-insulator transitions*, 2nd ed. Taylor and Francis, London, 1990.
- [11] T. Kolodiaznyy and S. C. Wimbush, *Phys. Rev. Lett.* 96 (2006) 246404(1–4).
- [12] R. D. Shannon, *Acta Crystallogr. A* 32 (1976) 751–767.
- [13] W. Jauch and A. Palmer, *Phys. Rev. B* 60 (1999) 2961–2963.
- [14] Q. Hui, M. G. Tucker, M. T. Dove, S. A. Wells, and D. A. Keen, *J. Phys.: Condens. Matter* 17 (2005) S111–S124.
- [15] G. H. Kwei, A. C. Lawson, S. J. L. Billinge, and S. W. Cheong, *J. Phys. Chem.* 97 (1993) 2368–2377.
- [16] T. Nakamura and S. Nomura, *Jpn. J. Appl. Phys.* 5 (1966) 1191–1196.
- [17] P. W. Anderson and E. Blount, *Phys. Rev. Lett.* 14 (1965) 217–219.
- [18] I. A. Sergienko, V. Keppens, M. McGuire, R. Jin, J. He, S. H. Curnoe, B. C. Sales, P. Blaha, D. J. Singh, K. Schwarz, and D. Mandrus, *Phys. Rev. Lett.* 92 (2004) 065501(1–4).